Title: Influence of Surface Pre-treatments on Laser Weldingof Ti6Al4V Alloy

J.M. Sánchez-Amaya[1,2], M.R. Amaya-Vázquez, L[1]. González-Rovira[1,2], M. Botana-Galvin[2], and F.J. Botana[1]

1. LABCYP, Departamento de Ciencia de los Materiales e Ingeniería Metalúrgica y Química Inorgánica, CASEM, Universidad de Cádiz, Campus Río San Pedro, 11510 Puerto Real (Cádiz), Spain;
2. Titania, Ensayos y Proyectos Industriales S.L. Parque Tecnológico TecnoBahía Edif. RETSE, Nave 4. Ctra. Sanlúcar Km 7, 11510 El Puerto de Santa María (Cádiz), Spain

Corresponding autor: e-mail: josemaria.sanchez@uca.es.

Abstract

In the present study, Ti6Al4V samples have been welded under conduction regime by means of a high power diode laser. The main objective of the work has been to determine the actual influence of the surface pre-treatments on the laser welding process. Thus, six different pre-treatments were applied to Ti6Al4V samples before performing bead-on-plate and butt welding treatments. The depth, width, microstructure, and microhardness of the different weld zones were deeply analyzed. Grinding, sandblasting, and chemical cleaning pre-treatments lead to welds with the highest depth values, presenting high joint strengths. Treatments based on the application of dark coatings generate welds with lower penetration and worse mechanical properties, specially the graphite-based coating.

Keywords laser beam welding, microstructure, surface treatments, Ti6Al4V

1. Motivation/State of the Art

Some interesting properties for welding of titanium alloys are their low thermal conductivity (lower than 22 W/cm/K), which prevents heat dissipation, and their low coefficient of thermal expansion (around 8.6 10^{-6}/m/m/K), which reduces thermal stresses during welding (Ref 1). Therefore, titanium alloys generally have low heat input, which minimizes welding stresses and reduces distortion (Ref 2). Titanium alloys also present a good rate of laser beam absorption (0.4%) and a high melting point (around 1670 °C) (Ref 1). These properties imply that high energy must be used to weld these alloys. Therefore, taking into account these considerations, laser welding technology is an adequate technology to join these alloys, as it allows a high localization and low size of the melting pool, reducing considerably the required energy in comparison with other welding technologies.

In other materials, such as aluminium alloys, various surface treatments such as sandblasting or the application of dark coatings are reported to improve the laser absorption, leading to significant increase of weld penetration (Ref 3-7). Different surface pre-treatments have been also applied to titanium alloys before welding in order to avoid surface oxidation and to improve laser absorption. Thus, in (Ref 1) a study focussed on improving laser beam absorption in TiG1 (commercially pure a titanium alloy) samples was carried out, concluding that sandblasted surfaces lead to the highest laser beam absorption, because they reduce the beam reflectivity. In other work (Ref 8), the influence of several surface preparations on the penetration of laser welds of commercially pure titanium has been studied. Black marker and air-abrasion pre-treatments are reported to lead to significantly deeper welds than mirror polished samples (Ref 8). Unfortunately, such kinds of studies are not available for other titanium alloys. In this context, there is not a clear consensus about the real influence of surface pre-treatments on laser welding process of Ti6Al4V titanium alloy, in terms of penetration, microstructure, and mechanical properties of the welds. The aim of the present paper has been to cover this gapof knowledge. Thus, the influence of different surface pre-treatments on the laser welding process of Ti6Al4V samples has been analyzed. In order to avoid the possible appearance of defects (such as porosities), the laser welding treatments have been performed with a high power diode laser (HPDL) under conduction regime. Six pre-treatments were applied to Ti6Al4V samples before performing bead-on-plate and butt welding treatments: ground at 80 grits (T1), sandblasted (T2), chemical cleaned (T3), painted with black marker (T4), painted with black spray paint (T5), and painted with graphite-based coating (T6). The beads size and shape (depth and width), the microstructure, and microhardness of the different zones were subsequently analyzed. Finally, tensile tests were performed on some welds to analyze the weld strength.

2. Experimental

Bead-on-plate and butt welding treatments were performed on Ti6Al4V samples using a HPDL under conduction regime (ROFIN-SINAR DL028S), working at the focal distance (69.3 mm from the focusing lens). The sample surface was always placed at the focus position, i.e., in all experiments the distance between the focussing lens and the samples surface was 69.3 mm. In this condition, the HPDL provides a spot size on surface of 2.2 9 1.7 mm2.

Figure 1 shows an image of this laser equipment, the mobile XY table, and the shielding gas system. The composition of the Ti6Al4V samples is shown in Table 1. Three types of welds were generated: bead-on-plate ofsmall samples (70 9 14 9 3 mm); butt welds of small samples (70 9 14 9 3 mm); and butt welds of bigger samples (50 9 50 9 3 mm, Fig. 2a), to obtain standard tensile speci-mens (Fig. 2b). Table 2 shows the six surface pre-treatments realized on Ti6Al4V samples before laser welding. Laser treatments consisted of a linear laser scan at a constant travel speed of 1 m/min and a power of 2500 W. Therefore, the power density (Irradiance) was 0.067 MW/cm^2 (laser power/area of the laser beam) and the fluence 6.82 KJ/cm^2 (laser power/welding speed 9 spot width) (Ref 6, 9). Big welded samples (for tensile tests) were performed with higher fluence to assurefull penetration (33 KJ/cm^2). The shielding gas was argon with a flow rate of 15 NL/min (NL are normal liters, i.e., liters measured in normal conditions, at 1 atm and 0 °C), applied with a conical coaxial nozzle (as shown in Fig. 1).

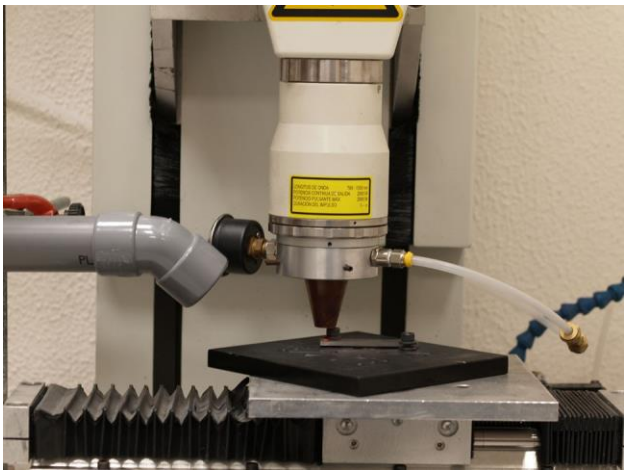

Fig. 1 High Power Diode Laser (HPDL) head, mobile XY table and shielding gas system

The beads size and shape (depth and width), the micro-structure, and the microhardness of the different zones were analyzed. For this study, mounted cross-sections of samples were evaluated, after polishing and etching for 10 s with Kroll's reagent (6 mL HNO_3, 2 mL HF, 92 mL H_2O). The morphology and size of the weld beads were analyzed with a Leica microscope (Model. MST53) controlled by LAS V4.2 software. As this software can correlate measured pixels and real distances of images, it allows the measurements of depth and width of the welds (calibrated equipments allowed one to verify this correlation). In order to assure the data accuracy, all welding experiments were performed in triplicate.

Scanning electron microscopy (SEM), x-ray energy-dispersive spectroscopy (EDS), and x-ray diffraction (XRD) were employed to analyze in detail the composition of some welds. EDS chemical analyses were performed using a Phoenix-EDAX equipment coupled at a SEM Quanta 200-FEI (FEI Company, Hillsboro, OR). XRD was performed by a Bruker instrument, model D8 Advance (radius 250 mm).

Microhardness measurements were accomplished with a Duramin microhardness tester of Struers, employing a charge of 2.945 N (0.3 HV). Finally, selected welds were subjected to tensile tests in a Shimadzu universal testing machine (100 kN) to evaluate the weld strength, fixing a deformation speed of 0.005 mm/min at the elastic deformation regime, and 1.6 mm/min at the plastic deformation regime. These tensile tests were

Table 2 Surface pre-treatments applied before laser welding

Surface pre-treatments	Identification
Sandblasted	T1
Ground at 80 grit	T2
Chemical cleaned	T3
Painted with black marker	T4
Painted with black spray paint	T5
Painted with graphite-based coating	T6

Table 1 Chemical composition of Ti6Al4V samples (wt.%)

Element	Al	V	Fe	C	Element remains, maximum %	Element remains, total %	Ti
Ti6Al4V	5.67	4.50	0.18	0.01	£ 0.10	£ 0.40	Balance

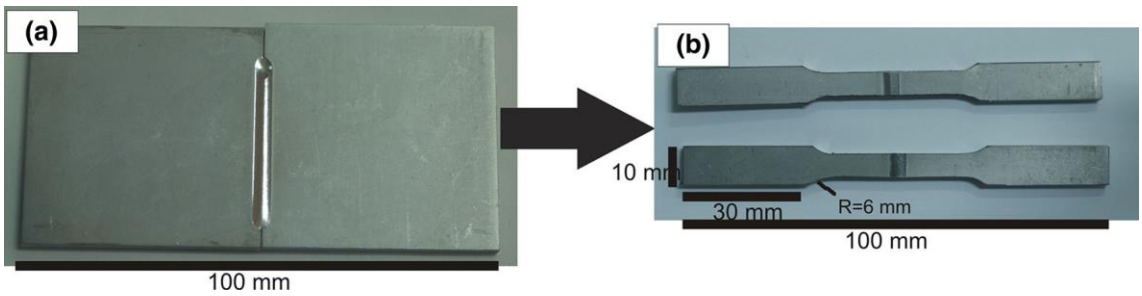

Fig. 2 Standard tensile specimens (b) obtained from butt welds (a)

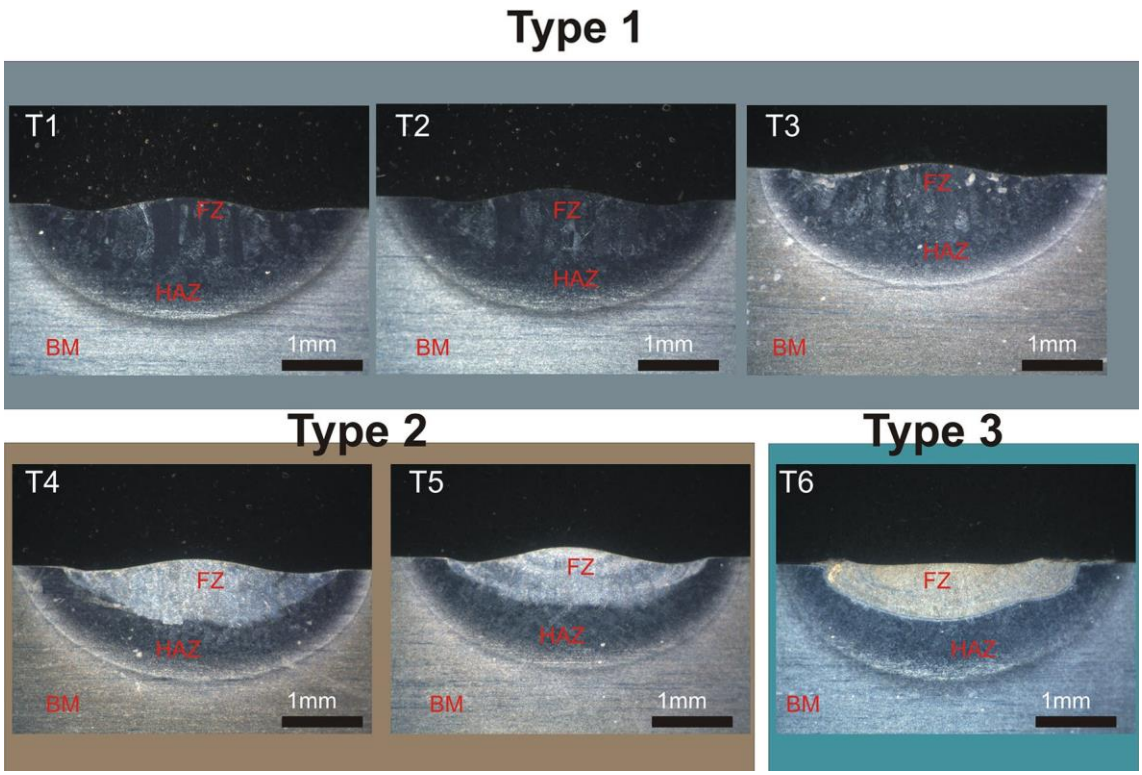

Fig. 3 Metallographic images at 309 of cross-sections of bead-on-plate weld beads

Table 3 Width and depth of bead-on-plate and butt welds

	Bead-on-plate				Butt welding			
	FZ + HAZ		FZ		FZ + HAZ		FZ	
Pre-treatments	Width, mm	Depth, mm	Width, mm	Depth, mm	Width, mm	Depth, mm	Width, mm	Depth, mm
T1	4.50 ± 0.08	1.73 ± 0.06	4.09 ± 0.08	1.21 ± 0.04	4.56 ± 0.16	1.69 ± 0.02	4.06 ± 0.22	1.23 ± 0.03
T2	4.400.03	1.72 ± 0.04	4.04 ± 0.05	1.25 ± 0.05	4.43 ± 0.20	1.71 ± 0.03	4.04 ± 0.19	1.27 ± 0.07
T3	4.70 ± 0.12	1.73 ± 0.01	4.28 ± 0.07	1.25 ± 0.06	4.79 ± 0.03	1.67 ± 0.05	4.36 ± 0.02	1.27 ± 0.04
T4	4.76 ± 0.03	1.74 ± 0.02	4.35 ± 0.09	0.93 ± 0.04	4.75 ± 0.12	1.61 ± 0.05	4.22 ± 0.03	0.93 ± 0.07
T5	4.74 ± 0.08	1.65 ± 0.10	4.29 ± 0.13	0.84 ± 0.01	4.72 ± 0.09	1.59 ± 0.12	4.26 ± 0.09	0.85 ± 0.10
T6	4.76 ± 0.09	1.67 ± 0.03	4.24 ± 0.03	0.83 ± 0.01	||| ||| ||| |||

performed on standard samples extracted from the welds (Fig. 2b), to fulfill the requirements of the ‘‘small size’’ specifications of ASTM E8/E8M-11.

3. Results and Discussion

3.1 Size and Shape of Bead-On-Plate and Butt Welds

Metallographic images at low magnification (309) of bead-on-plate beads cross-sections are included in Fig. 3. Regardless of the applied pre-treatment, three different zones are always identified: the fusion zone (FZ), the heat-affected zone (HAZ), and the base metal (BM). In both bead-on-plate and butt welding experiments, the weld shape is always close to a semicircle, allowing one to confirm that the weld beads are always generated under conduction regime. As can be seen in the metallographic images, this regime gives rise to beads with

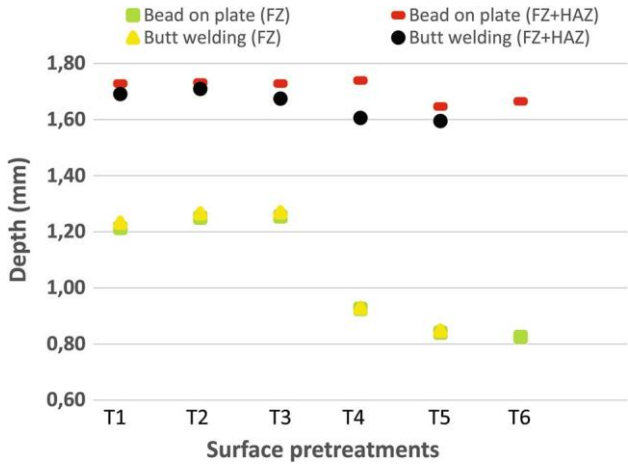

Fig. 4 Depth of (FZ + HAZ) and (FZ) of bead on plate and butt welding

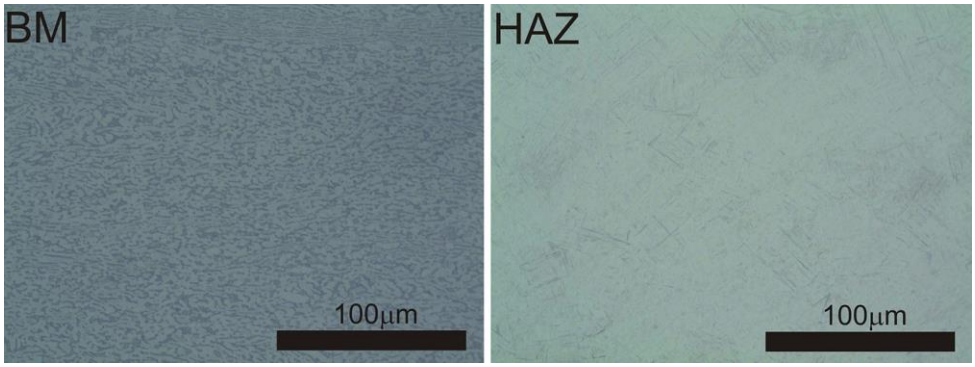

Fig. 5 Examples of metallographic images (at 500ϑ) of BM and HAZ of the welded samples

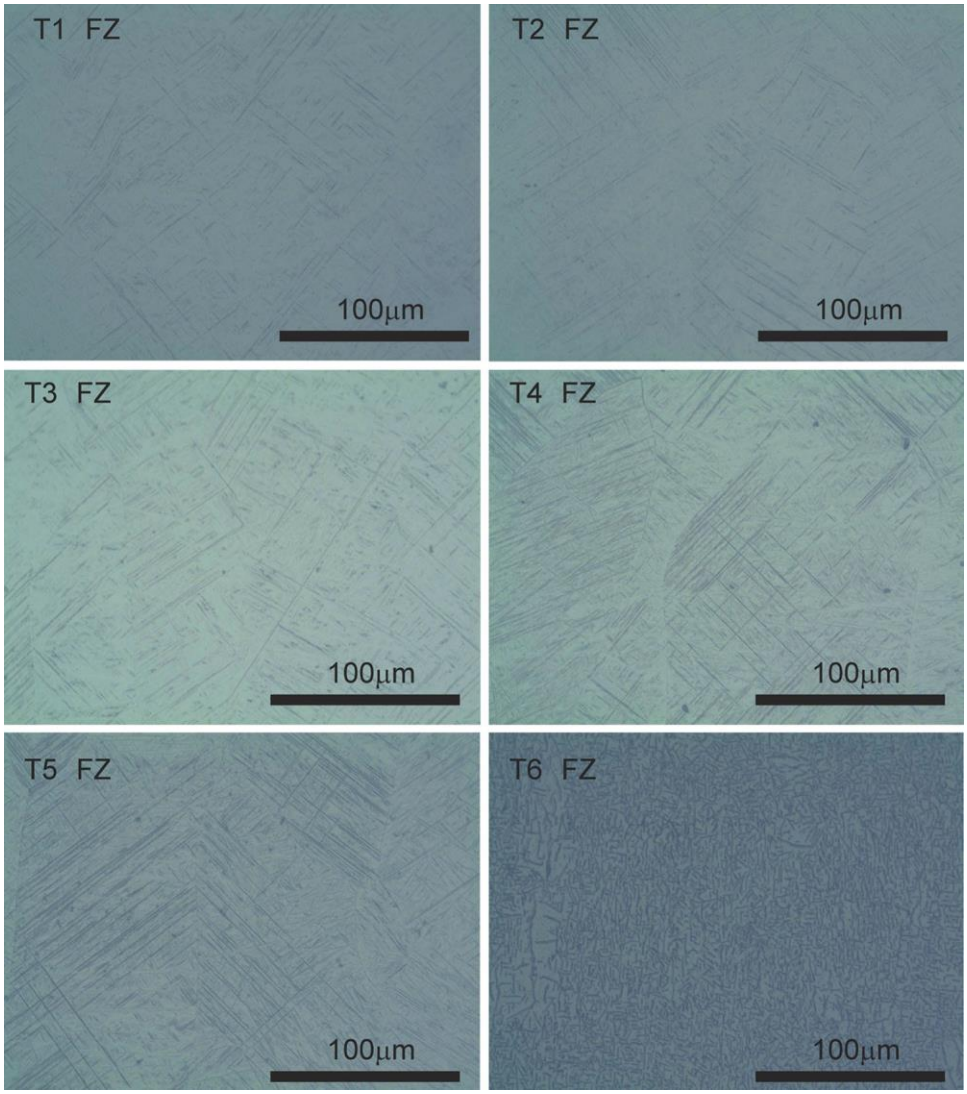

Fig. 6 Metallographic images (at 500ϑ) of FZ of bead-on-plate beads obtained with different surface pre-treatments

much lower porosity than the weld beads that are usually obtained under keyhole regime (Ref 1, 6, 9-11).

Table 3 reports the depth and width values of the obtained welds (bead-on-plate and butt welds). In order to analyze the welds in detail, data (depth and width) from fusion zone only (FZ) and data from the whole heat-affected zone (includingFZ + HAZ) are reported in Table 3. The average and the standard deviation values included in Table 3 have been

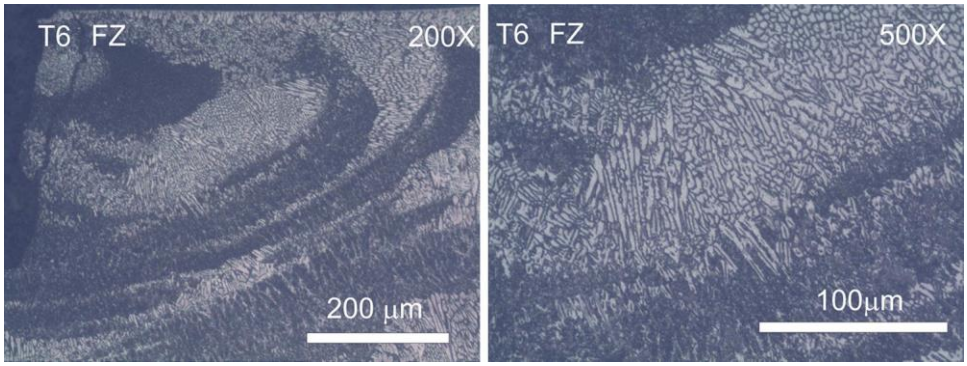

Fig. 7 Metallographic images (at 200ϑ and 500ϑ) of FZ of broken T6 butt weld

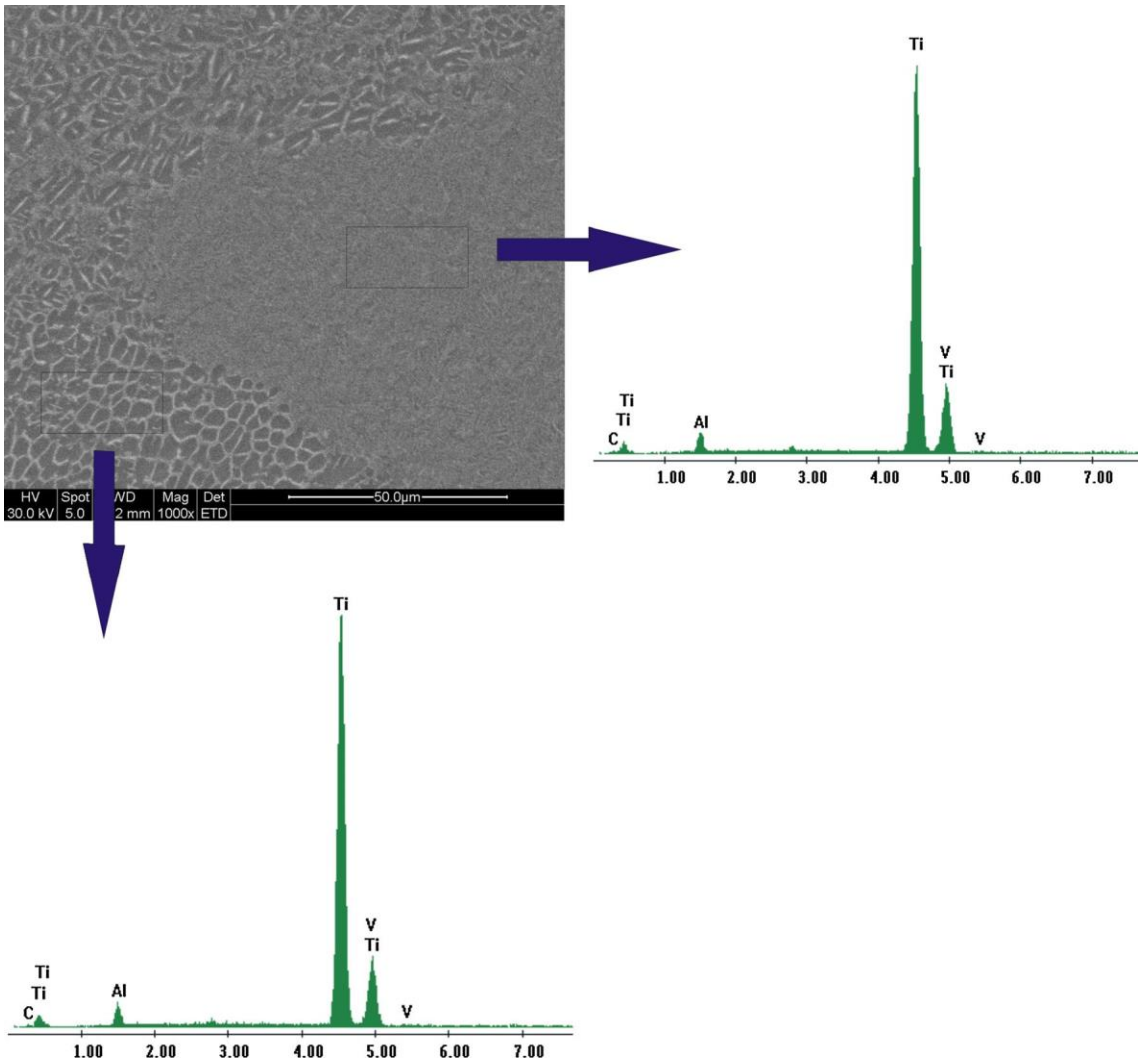

Fig. 8 SEM and EDS of FZ of broken T6 butt weld

estimated from the analysis of three welds obtained in each condition.

Figure 4 plots the averaged penetration of the FZ and FZ + HAZ of the different welds. As expected, the depths of the bead-on-plate samples present the same tendency than the butt welds, showing also similar penetration values. The depths of the whole heat-affected zone (FZ + HAZ) are observed to be similar in all welds, regardless of the surface treatment. However, the penetration values of the FZ are clearly different for each treatment. According with the microstructure anddepth of the FZ (Fig. 3, 4), the welds can be classified into threetypes: Type 1 corresponding to pre-treatments T1, T2, and T3;

Type 2 corresponding pre-treatments T4 and T5; and finally Type 3, corresponding to pre-treatment T6. The deepest FZ is obtained in Type 1 welds (sandblasted, ground and chemical cleaned samples), reaching penetration values between 1.2 and 1.3 mm. Type 2 welds (with treatments based on application of black coatings) presented FZ with lower penetrations (0.8-1.0 mm) than Type 1 welds. Finally, Type 3 welds (with graphite-based coating) showed the lowest values (0.8-0.9 mm). Note that the depths of the butt welds of this latter treatment are not reported because they broke during the metallographic preparation.

In summary, samples with treatments T1, T2, and T3 have the deepest FZ, meaning that the effective heat input within the laser welding is higher than that involved in samples with treatments T4, T5, and T6. The higher heat input provokes higher temperatures in the weld pool, and consequently, greater FZs. The relatively high heat transfer in T1 and T2 is thought to be due to the high roughness of the surfaces (encouraging the energy absorption), while in the case of T3, the reason seems to be related to a cleaning effect (the chemical cleaning dissolve oxides and others contaminants from surface, increasing the direct laser absorption). Samples with treatments T4, T5, and T6 seem to receive lower effective heat input, probably because of the ablation of the coatings applied to the surface.

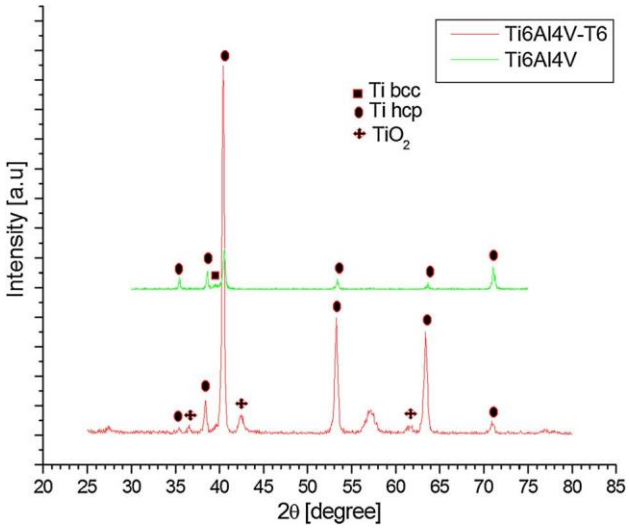

Fig. 9 XRD of FZ of broken T6 butt weld

Accordingly, the evaporated coatings material can react with the incoming laser source and generate plasma, which can absorb part of the beam energy. This process reduces the effective energy received by the sample to generate the weld pool. As a consequence, the temperatures of the liquid welds in T4, T5, and T6 samples would be lower than in T1, T2, and T3 samples, leading to smaller melting pools and, therefore, to smaller FZ.

3.2 Microstructure of Bead-On-Plate and Butt Welds

Figure 5 includes the typical metallographic images (at 500) of BM and HAZ of the welded samples. Similar microstructure is observed in all bead-on-plate and butt welds obtained with the six pre-treatments. In agreement with (Ref 9, 12), the microstructure of Ti6Al4V BM is observed to consist of inter-granular beta phase (b, BCC structure) in an equiaxed alpha phase (a, HCP structure). Meanwhile, the HAZ microstructure consists of a mixture of martensitic a¢ and primary a.

Figure 6 reports metallographic images at high magnification (500X) of the FZ of bead-on-plate welds obtained with the different pre-treatments. The FZ microstructures of all samples (including bead-on-plate and butt welds) are identified as a¢ martensite (microhardness values presented later support the identification of martensite). Martensitic phase could be obtained because the welding pool temperature reached the b transus (980 °C for Ti6Al4V) and the cooling rate was higher than 410 °C/s (Ref 13, 14). A careful observation of the images allows to state that some differences can be found between the martensitic microstructure of the six pre-treatments. Thus, FZ of T1, T2, and T3 (Type 1) consists of acicular a¢ martensite, microstructure similar to that obtained by authors in previous work (Ref 9). Both T4 and T5 (Type 2) presented a plate-like martensitic microstructure with a higher density of dark acicular particles than T1-T3. These darker particles are also present at grain boundaries located inside the FZ of T4 and T5 samples. FZ of T6 samples (Type 3) is clearly different from the others; small dark elongated zones are extensively incorporated to the martensite microstructure. Deeper analyses were performed to this sample in order to evaluate the possible formation of TiC or graphite inclusions (Ref 15), as these particles can provoke important welding embrittlement. In fact, butt welds of T6 could not be obtained because they broke easily. Micrographs of butt welds of T6 broken samples can be observed in Fig. 7. Figure 8 and 9 report the results of the analyses performed by SEM-EDS and XRD. The EDS spectra (Fig. 8) did not detect the presence of carbon, while x-ray

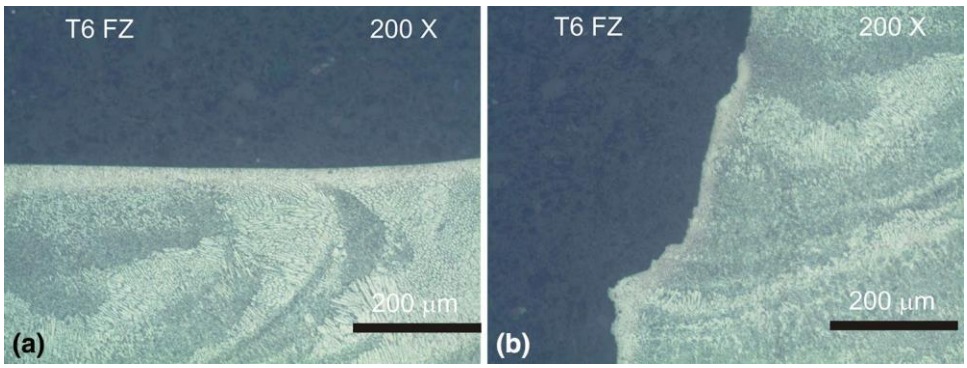

Fig. 10 Metallographic images (at 200) of broken T6 butt weld

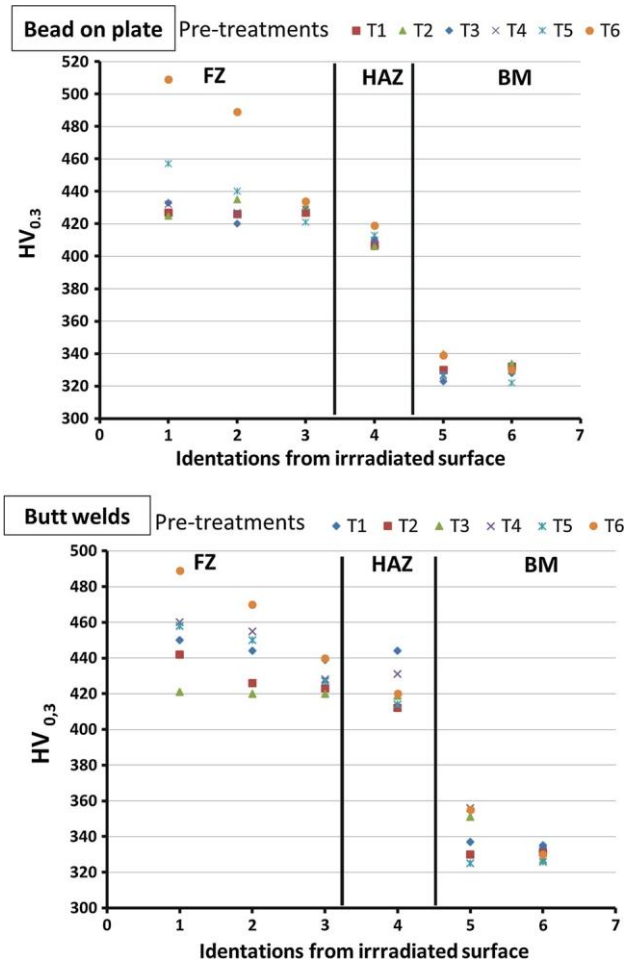

Fig. 11 Microhardness profiles of bead-on-plate and butt welds in function of the surface pre-treatment

diffractograms (Fig. 9) only revealed the presence of TiO_2. Therefore, neither TiC nor graphite was detected in T6 butt weld sample. The reason of the premature failure of the weld is thought to be due to the formation of alpha case. Besides the TiO_2 layer, an alpha case layer can be clearly observed in metallographic images included in Fig. 10. Alpha case is an oxygen-enriched layer, hard, brittle, and considered detrimental (Ref 16). This undesirable superficial microstructure is normally formed in titanium alloys when exposed to air at temperatures higher than 540 °C (813 K).

3.3Microhardness Profile of Bead-On-Plate and Butt Welds

Figure 11 reports the microhardness profile of both bead-on-plate and butt welds. As expected, in all samples, FZ has higher microhardness values than HAZ and BM, as a consequence of the martensitic formation. T6 treatment is observed to provide the hardest FZ microstructure, probably due to the dark elongated zones incorporated to the martensite microstructure (Fig. 6).

3.4 Strength of Selected Butt Welds

Standard specimens were extracted from Type 1 butt welds, as shown in Fig. 2, to fulfill the requirements of ASTM E8/ E8M-11. Tensile tests were performed to these samples and

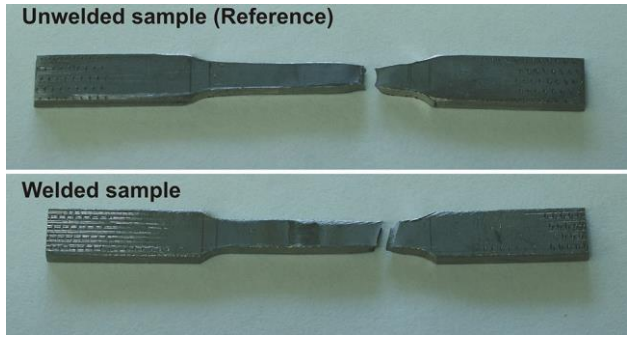

Fig. 12 Tensile specimens after tests

also to BM probes, with the aim of verifying that the strength of the welded sample is similar to the reference untreated sample (BM). Yield strength (YS) and ultimate tensile strength (UTS) values were estimated from the tests. Similar values for both parameters were obtained (Untreated Sample: YS = 990 ± 8 MPa, UTS = 1058 ± 9 MPa; Weld: YS = 914 ± 17 MPa, UTS = 1050 ± 20 MPa). Images of broken samples are in- cluded in Fig. 12. Welded samples break at the BM, far from the joint. According to these results, it can be stated that weldedsamples are as strong as the reference unwelded sample, as theyshow similar strength values (in fact, the welded sample brokeat the BM, confirming that the HAZ and FZ are stronger than the BM in the welded samples).

4. Conclusions

In the present study, the influence of the surface pre-treatments on the laser welding process of Ti6Al4V samples has been analyzed. Six different pre-treatments were studied as follows: ground at 80 grit (T1), sandblasted (T2), chemical cleaned (T3), painted with black marker (T4), painted with black spray paint (T5), and painted with graphite-based coating (T6). The beads size and shape (depth and width), the microstructure, and the microhardness of the different zones were analyzed. Although martensite was detected in the FZ of all welds, the detailed microstructure and microhardness of welds are sensitive to the surface pre-treatment. T1 to T3 leaded to the welds with the deepest FZ, presenting also similar strength in tensile tests than reference unwelded samples. Treatments involving the application of dark coatings lead to welds with lower penetration and worse mechanical properties, especially T6, which provoke weld hardening and embrittlement.

References

1. C. Bertrand, O. Laplanche, J.P. Rocca, Y. Le Petitcorps, and S. Nammour, Effect of the Combination of Different Welding Parameters on Melting Characteristics of Grade 1 Titanium with a Pulsed Nd-YagLaser, *Lasers Med. Sci.*, 2007, 22, p 237–244
2. A. Costa, R. Miranda, L. Quintino, and D. Yapp, Analysis of Beam Material Interaction in Welding of Titanium with Fiber Lasers, *Mater.Manuf. Process.*, 2007, 22, p 798–803
3. P. Okon, G. Dearden, K.Watkins, M. Sharp, and P. French, Laser Welding of Aluminium Alloy 5083, *21st International Congress on Applications of Lasers and Electro-Optics*, Scottsdale, Oct 14-17,(ICALEO 2002) ISBN 0-912035-72-2

4. W.W. Duley, *Laser Welding, Chapter 4*, Wiley, New York, 1999, p 69
5. K. Howard, S. Lawson, and Y. Zhou, Welding Aluminium Sheet Usinga High-Power Diode Laser, *Weld. J.*, 2006, 85(5), p 101–110
6. J.M. Sánchez-Amaya, T. Delgado, J.J. De Damborenea, V. López, and F.J. Botana, Laser Welding of AA 5083 Samples by High Power DiodeLaser, *Sci. Technol. Weld. Join.*, 2009, 14(1), p 78–86
7. J. Oñoro, R. Bermejo, and Y.L. Sánchez-Ibarzabal, Análisis de la influencia del estado superficial en la energ´ıa absorbida en la interacción láser CO_2-aluminio, *Rev. Met. Madrid*, 2005, 41, p 40–45
8. I. Watanabe, N. Baba, J. Chang, and Y. Chiu, Nd:YAG Laser Penetration into Cast Titanium and Gold Alloy with Different SurfacePreparations, *J. Oral Rehabil.*, 2006, 33, p 443–446
9. M.R. Amaya-Vázquez, J.M. Sánchez-Amaya, Z. Boukha, and F.J. Botana, Microstructure, Microhardness and Corrosion Resistance of Remelted TiG2 and Ti6Al4V by a High Power Diode Laser, *Corros. Sci.*, 2012, 56, p 36–48
10. J.M. Sánchez-Amaya, T. Delgado, L. González-Rovira, and F.J. Botana, Laser Welding of Aluminium Alloys 5083 and 6082 Under Conduction Regime, *Appl. Surf. Sci.*, 2009, 255(23), p 9512–9521
11. T.Y. Kuo and H.C. Lin, Effects of Pulse Level of Nd-YAG Laser on Tensile Properties and Formability of Laser Weldments in AutomotiveAluminium Alloys, *Mater. Sci. Eng. A Struct.*, 2006, 416, p 281–289
12. E. Akman, A. Demir, T. Canel, and T. Sınmazcelik, Laser Welding of Ti6Al4V Titanium Alloys, *J. Mater. Process. Technol.*, 2009, 209,p 3705–3713
13. X. Cao and M. Jahazi, Effect of Welding Speed on Butt Joint Quality of Ti-6Al-4V Alloy Welded Using a High-Power Nd:YAG Laser, *Opt. Laser Eng.*, 2009, 47, p 1231–1241
14. T. Ahmed and H.J. Rack, Phase Transformations During Cooling in a + b Titanium Alloys, *Mater. Sci. Eng. A*, 1998, 243, p 206–211
15. A.F. Saleh, J.H. Abboud, and K.Y. Benyounis, Surface Carburizing of Ti-6Al-4V Alloy by Laser Melting, *Opt. Laser Eng.*, 2010, 48, p 257– 267
16. J.M. Sanchez-Amaya, M.R. Amaya Vázquez, and F.J Botana, *Hand- book of Laser Welding Technologies. Chapter 8 Laser Welding of LightMetal Alloys: Aluminium and Titanium Alloys*. S. Katayama, Eds., Osaka University, Japan. Woodhead Publishing Series in Electronic and Optical Materials No. 41, p 215–254